

Status of AlGaIn/GaN HEMT Technology-A UCSB perspective

Umesh K. Mishra
ECE Department,
UCSB, Santa Barbara, CA 93106
Funded by ONR, AFOSR and DARPA

The following major technological advances

- (i) the ability to grow high quality materials on sapphire and SiC,
- (ii) the advent of SiN passivation to eliminate current slump or dispersion,
- (iii) advanced processing, and
- (iv) implementation of field plates

have taken AlGaIn/GaN HEMTs to commercialization in the relatively short time of approximately a decade. In this paper we will present the highlights of this research and a small window (by no means complete) into the future.

Prior to the introduction of field plates the power density available from GaN-based HEMTs was in the range of order of 10-11W/mm as demonstrated by CREE and Cornell University. These devices were fabricated on high quality material on SiC grown by MOCVD with a dislocation density of $<10^9$ cm⁻². The advent of field plates changed the rate of advance in a disruptive fashion. Field plates come in two flavors. One is an integrated field plate where the definition of the gate defines the field plate extension as shown in figure 1a. The second is a separately defined plate such as shown in figure 1b which can be connected either at the drive point of the gate (single ended) or at both ends of the gate. This second implementation has enhanced flexibility (of course at the cost of additional process steps). The separate field plate could be multiple in numbers or could be connected to the source as examples of this flexibility.

The first clear demonstration of the impact of field plates was by Chini *et. al.* (UCSB) when the addition of a single separate field plate increased the device performance from 8 W/mm to 18.8W/mm, as shown in figure 2a. The enhancement in the performance was due to the reduction of the peak field at the edge of the drain-edge of the gate. This enabled both a *higher operating voltage* of the HEMT and a *reduced dispersion* which led to higher power added efficiencies. The second advantage is critical in GaN-based devices where dispersion is the main factor in determining large signal device performance. Optimization of the field plate by Wu *et. al.* (CREE) has led to a record device power density of 32W/mm at 4GHz, as shown in figure 2b. The price that one pays for these enhancements is the additional C_{GD} in gate-connected field plates. The optimization of the field plate length is therefore dependent on application (frequency and voltage).

The first demonstration of the use of multiple field plates was performed by Karmalkar and Mishra (theory) and Xing *et. al.* (experiment) at UCSB. The application focus of this implementation was the development of high voltage HEMTs with breakdown voltage in

600V to 1 kV range for switched power converters. Figure 3 shows the implementation which demonstrated AlGaIn/GaN HEMTs with 900V breakdown voltage with 3 field plates.

To mitigate the detrimental effect of enhanced C_{GD} , Wu *et al.* (CREE) implemented source-connected field plates as shown in figure 4. C_{GD} was reduced substantially, even compared with non-field-plated devices. This resulted in a dramatic enhancement in the gain of the devices at 4 GHz.

A legitimate question arises: Now what? It is our opinion that in addition to improvements in reliability and manufacturability we will see advanced designs that are relatively insensitive to passivation, rapid advances in the application of AlGaIn/GaN HEMTs at mm-wave frequencies, and potentially the exploitation of N-face growth for unique device structure implementation.

Deeply Recessed Devices: Shen et al. (UCSB) first demonstrated that a device employing a deep recess to separate the surface from the channel mitigated in a controlled fashion the electrostatic impact of the charging and discharging of surface states, or dispersion. These devices demonstrated excellent performance in the absence of passivation as shown in figure 5.

mm-wave Devices: Palacios et al. (UCSB) have recently shown excellent performance using AlGaIn/GaN HEMTs at mm-wave frequencies. The use of novel device structures to enhance the confinement of the electrons in the channel (Figure 6), in combination with very short channel transistors (<100 nm) and high breakdown voltages has allowed the fabrication of AlGaIn/GaN HEMTs with output power densities in excess of 10 W/mm at 40 GHz with power added efficiencies higher than 30% (Figure 7). These results will improve even further by drastically reducing the parasitic capacitances and resistances in these devices. For example, in preliminary experiments in devices with low parasitic capacitances, current cut-off frequencies in excess of 150 GHz and power gain frequencies of more than 230 GHz have already been demonstrated (see Figure 8). When correctly optimized for power, these devices are expected to render outstanding power performance at Ka-band and above.

N-face AlGaIn/GaN HEMTs: GaN research in the past has mainly focused on Ga-polar devices, and N-face GaN buffers, electronic devices based on structures grown in the N-face (0 0 0 $\bar{1}$) polarity have not been explored in much detail in the past. Several new device structures with potential advantages over Ga-face HEMTs can be designed in the N-face orientation as demonstrated by Rajan et al (UCSB). An enhancement-mode device can be created by etching the AlGaIn in the access regions of an N-face GaN-buffer/AlGaIn/GaN/AlGaIn device. The advantage of using N-face GaN is that the access region etch is not critical to device performance as opposed to gate recess etching that is necessary for a Ga-face enhancement mode device. Gate leakage is an important issue for GaN-based high power devices. In a N-face device with a GaN-buffer/AlGaIn/GaN/thin-AlGaIn, the electrostatics can be designed so that the electric field in the top AlGaIn layer

is lowered as the negative gate bias is increased, thus reducing the gate leakage. In addition it is also possible to create low dispersion devices in N-face orientation.

The structures were grown by plasma-assisted MBE on CMP-polished (NovaSiC) 6H C-face SiC. The threading dislocation density was $2 \times 10^{10} \text{ cm}^{-2}$ with surface roughness less than 1 nm. The polarity was determined to be N-face from 3x3 RHEED reconstructions, etching in basic solutions, and CV measurements.

In the modulation-doped HEMT sample grown, the structure consisted of a GaN buffer followed by 20 nm $\text{Al}_{0.3}\text{Ga}_{0.7}\text{N}:\text{Si}$ doped at 3×10^{18} , 10 nm undoped $\text{Al}_{0.3}\text{Ga}_{0.7}\text{N}$, and 30 nm undoped GaN. A Hall sheet charge density of $7.8 \times 10^{12} \text{ cm}^{-2}$ with a mobility of $950 \text{ cm}^2 \text{ V}^{-1} \text{ s}^{-1}$ was measured. TLM, Hall and CV measurements were found to be consistent. Transistors had a maximum current density of 1 A/mm and a pinch-off voltage of 6 V. Surface dispersion was reduced using SiN passivation and f_T and f_{max} were found to be 20 GHz and 45 GHz respectively. Enhancement-mode operation was also achieved in other structures based on a channel-recess design. Currents of up to 100 mA/mm were achieved in these structures with a threshold of 0.5 V.

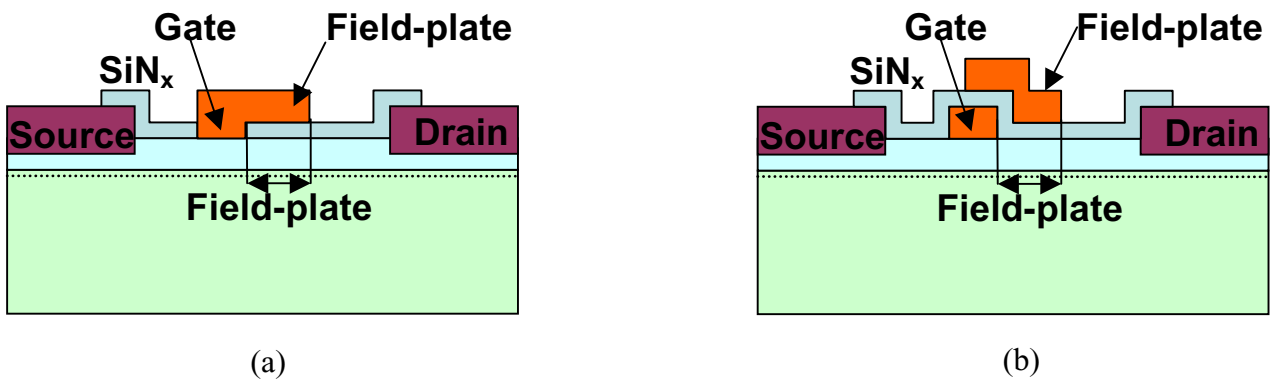


Figure 1. Field-plated AlGaIn/GaN HEMTs (a) integrated field plate; (b) separated field plate.

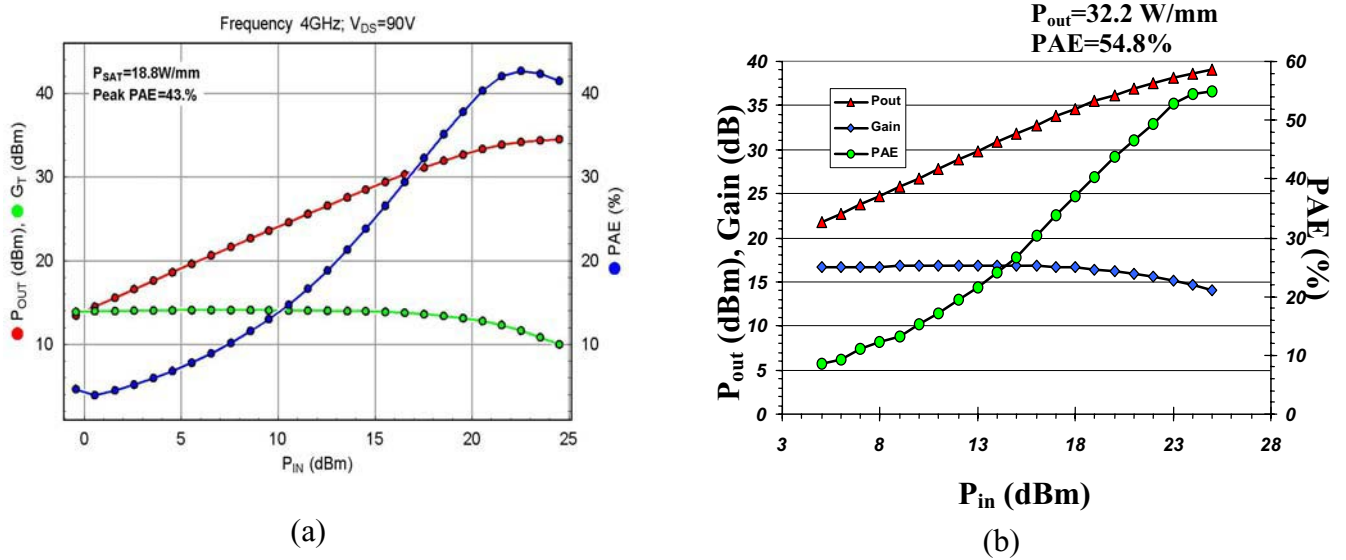
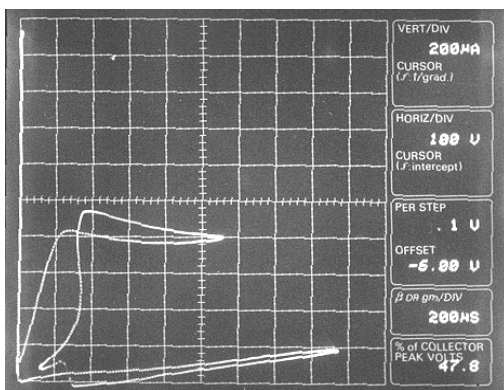
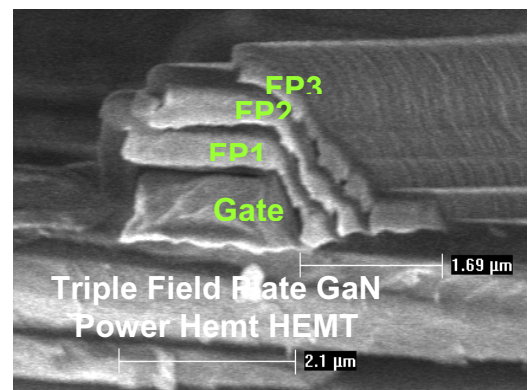


Figure 2. Power performance of field-plated AlGaIn/GaN HEMTs. (a) 18.8W/mm with PAE 43% at V_{DS} of 90V; (b) 32.2W/mm with PAE 55% at V_{DS} of 120V.



(a)



(b)

Figure 3. Multiple field plates, high breakdown AlGaIn/GaN HEMTs. (a) high breakdown voltage of 900V; (b) SEM image of the cross-section of multiple field plates.

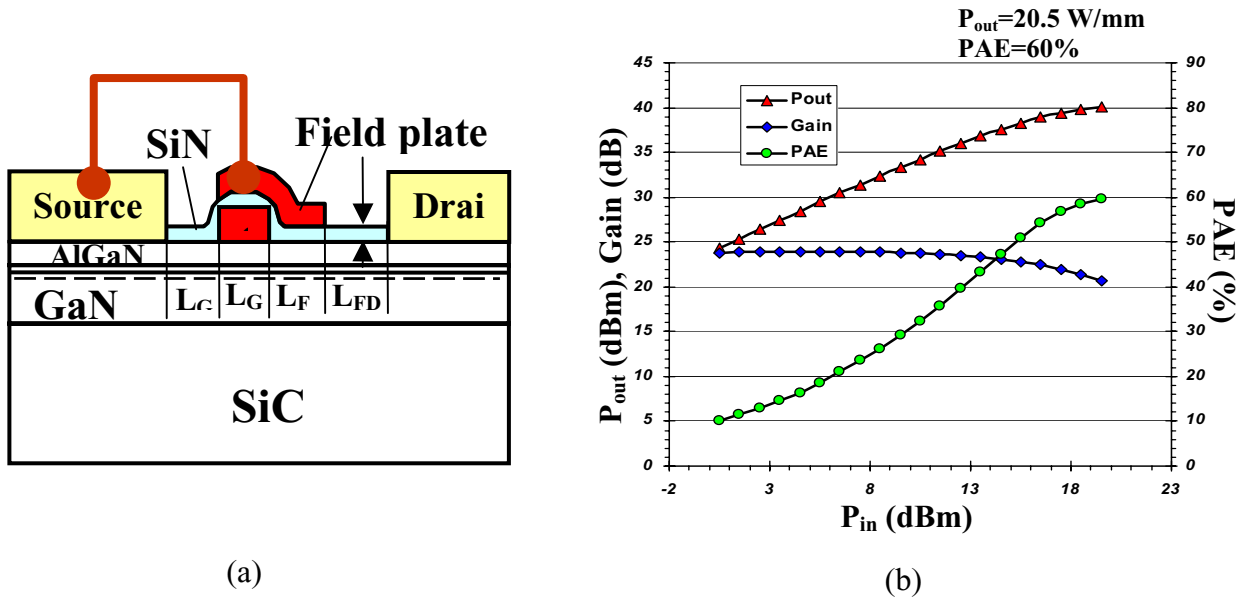


Figure 4. Source-terminated field-plate AlGaN/GaN HEMTs. (a) Schematic of cross-section; (b) 20.5W/mm with 60% PAE at 4GHz. Linear gain is 24dB and larger signal gain is 21dB.

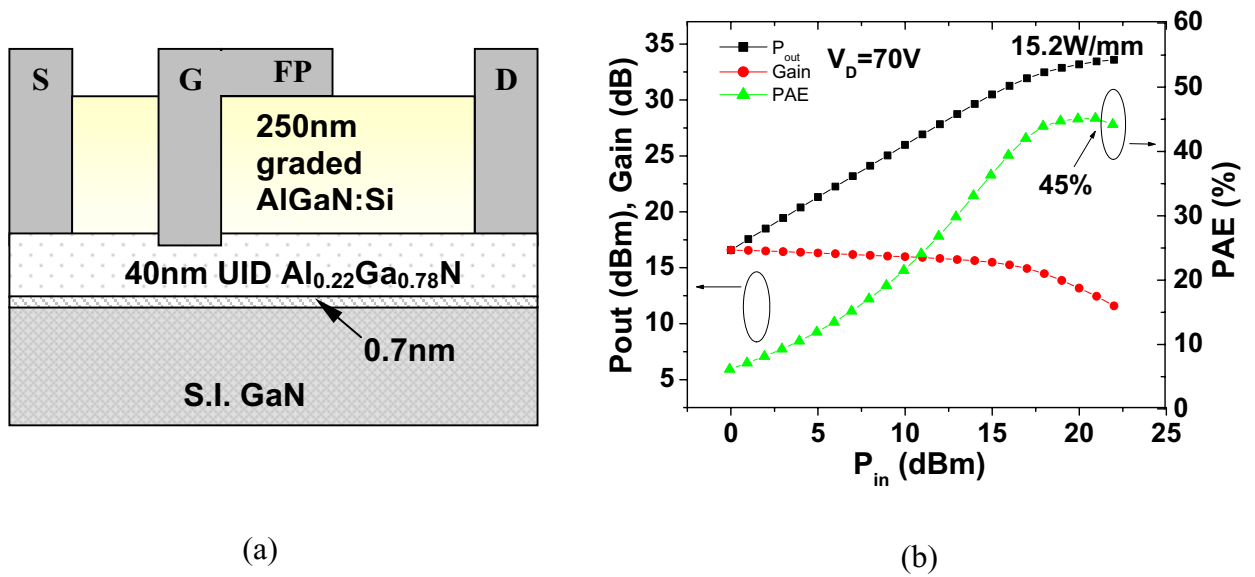
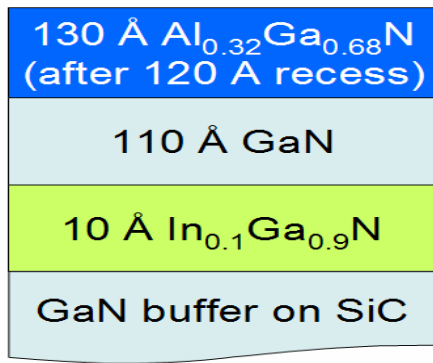
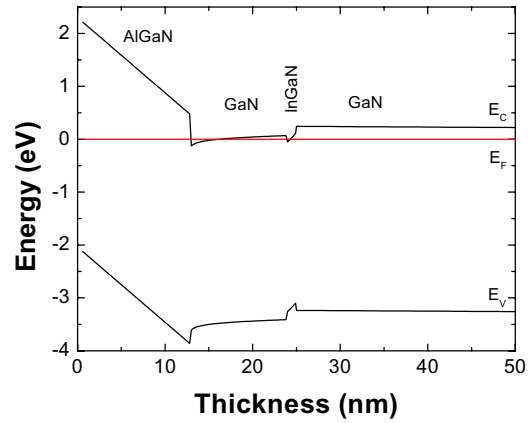


Figure 5. Deep-recessed GaN-based HEMTs. (a) Schematic of cross-section; (b) Power performance of the deep-recessed HEMT at 4GHz with no surface passivation.



(a)



(b)

Figure 6. Structure of an AlGaN/GaN HEMT with an InGaN back-barrier to increase the confinement of the electrons in the channel.

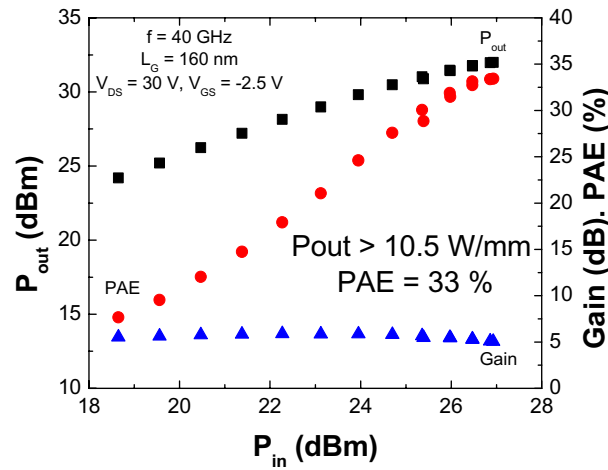
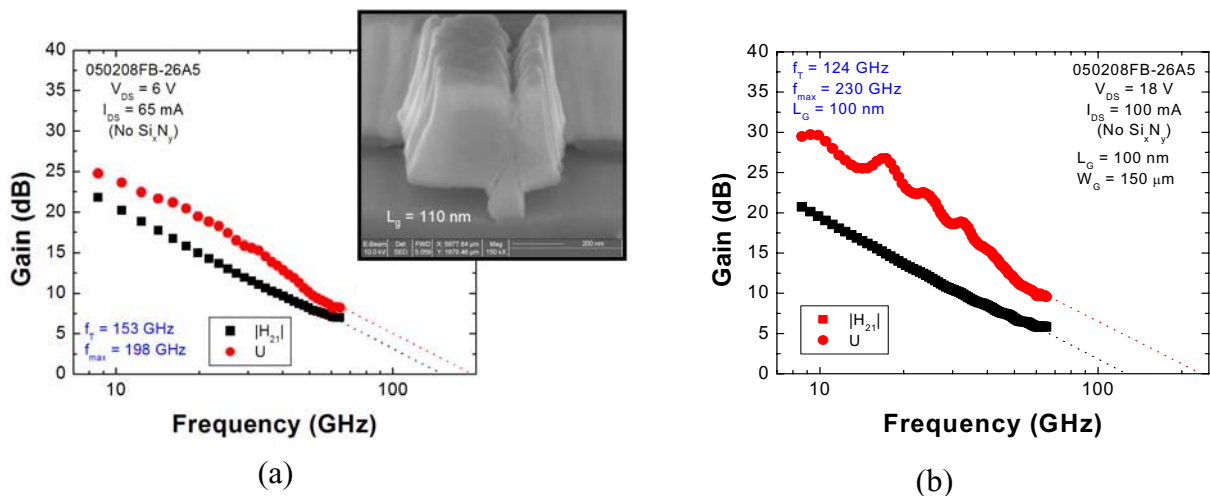


Figure 7. Power saturation plot of an AlGaN/GaN HEMT at 40 GHz.



(a)

(b)

Figure 8. Extrinsic small-signal high-frequency performance of an optimized AlGaN/GaN HEMT.

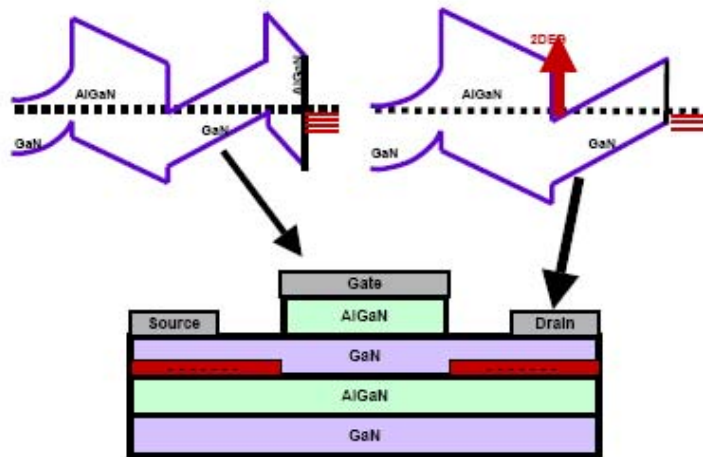


Figure 9. Band diagram of enhancement mode device. The 2DEG is depleted beneath the gate at zero bias.

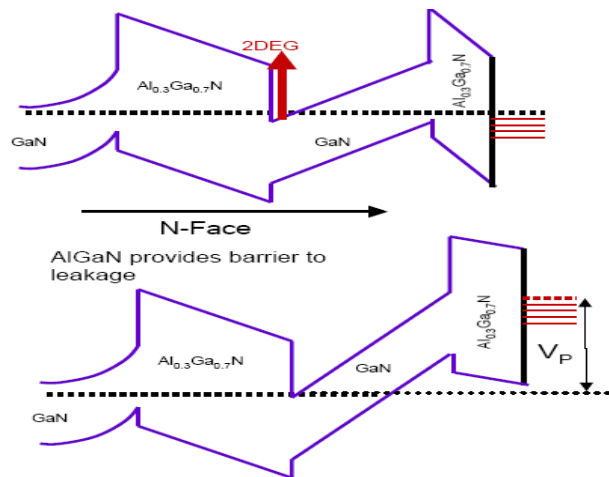


Figure 10. Low Gate Leakage: N-face AlGaN/GaN/AlGaN transistor. As the device is pinched off, the conduction band in the top AlGaN approaches flat-band leading to low gate leakage.

